Inorganic Chemistry

Article

pubs.acs.org/IC

Metal Complexes of Bridging Neutral Radical Ligands: pymDTDA and pymDSDA

Jian Wu,[†] Daniel J. MacDonald,[†] Rodolphe Clérac,[‡,§] Ie-Rang Jeon,[‡,§] Michael Jennings,[⊥] Alan J. Lough,[¶] James Britten,[∥] Craig Robertson,[∥] Paul A. Dube,[Δ] and Kathryn E. Preuss*[,†]

[†]Department of Chemistry, University of Guelph, Guelph, Ontario N1G 2W1, Canada

[‡]Centre de Recherche Paul Pascal (CRPP), Equipe "Matériaux Moléculaires Magnétiques", 115 avenue du Dr. Albert Schweitzer, Pessac F-33600, France

[§]Université de Bordeaux, UPR 8641, Pessac F-33600, France

[⊥]Department of Chemistry, The University of Western Ontario, London, Ontario N6A 5B7, Canada

[¶]Department of Chemistry, University of Toronto, Toronto, Ontario M5S 3H6, Canada

[∥]Department of Chemistry, McMaster University, Hamilton, Ontario L8S 4M1, Canada

[Δ]Brockhouse Institute for Materials Research (BIMR), McMaster University, Hamilton, Ontario L8S 4M1, Canada

Supporting Information

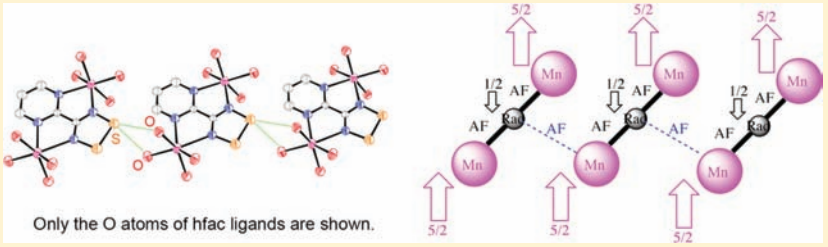

ABSTRACT: Metal complexes of the 4-(2′-pyrimidyl)-1,2,3,5-dithiadiazolyl (pymDTDA) neutral radical ligand and its selenium analogue (pymDSDA) are presented. The following series of metal ions has been studied using $M(hfac)_2$ as the coordination fragment of choice (hfac = 1,1,1,5,5,5-hexafluoroacetylacetonato): Mn^{II}, Co^{II}, Ni^{II}, and Zn^{II}. The binuclear cobalt and nickel complexes of pymDTDA both exhibit ferromagnetic (FM) coupling between the unpaired electrons on the ligand and the metal ion, while the binuclear zinc complex of pymDTDA is presented as a comparative example incorporating a diamagnetic metal ion. The binuclear manganese complex of pymDTDA, reported in a preliminary communication, is compared to the pymDSDA analogue, and new insight into the magnetic behavior reveals that intermolecular magnetic coupling, mediated by chalcogen−oxygen contacts, gives rise to a significant increase in the χT product at low temperature. Surprisingly, the binuclear nickel complex of pymDSDA forms dimers in the solid state, as do the mononuclear complexes of cobalt and nickel with pymDTDA. In addition, mixed mononuclear/binuclear complexes of Mn- and Zn(pymDTDA) have been identified.

INTRODUCTION

One of the most important factors in the design, development, and progress of molecular and supramolecular metal chemistry is the availability of ligands with specific geometric, chemical, and electronic features. Whether the goal is to create a better model complex of a metal-containing enzyme or to develop new photosensitizing dyes for solar cell technology, increasing the diversity of available metal and ligand "building blocks" can play a critical role.

Our aim is to explore the use of known thiazyl and selenazyl radicals for the design of new ligands. By combining "classic" organic ligand architectures with well-developed main-group structures, we endeavor to contribute a variety of novel ligands with unusual and potentially useful properties. This approach has afforded neutral radical ligands that have metal chelation "pockets" analogous to 2,2′-bipyridine and 2,2′-bipyrimidine. The metal complexes of the former are described elsewhere in the literature.[1−4] Herein, we describe the structural and magnetic properties of metal complexes of the latter, 4-(2′-pyrimidyl)-1,2,3,5-dithiadiazolyl (pymDTDA; **1a**; Chart 1) and 4-(2′-pyrimidyl)-1,2,3,5-diselenadiazolyl (pymDSDA; **1b**). A preliminary report has demonstrated that radical ligand **1a** can chelate two Mn^{II} centers and that antiferromagnetic (AF) coupling between the metal and ligand spins results in an overall ferrimagnetic spin arrangement with an $S_T = {}^9/_2$ spin ground state per molecule.[5] Herein, a structural and magnetic investigation of the binuclear complexes of **1a** with paramagnetic metal ions Ni^{II} and Co^{II} is presented (complexes **2a** and **3a**, respectively). Ferromagnetic (FM) coupling between the metal and ligand spins is observed in both cases. In addition, we present new insight into the magnetic behavior of

Received: January 5, 2012
Published: February 17, 2012

   dx.doi.org/10.1021/ic3000284 | *Inorg. Chem.* 2012, 51, 3827−3839

Chart 1

the previously reported binuclear manganese(II) complex **4a**; specifically, the reproducible, and previously unaccounted for, observation of a significant increase in the χT product at low temperature is discussed. The binuclear zinc(II) complex **5a** represents the first example of N-coordination of a DTDA ligand with a diamagnetic metal ion and serves to illustrate the properties of the coordinated radical ligand in the absence of any other source of paramagnetism. Binuclear coordination species of the selenazyl ligand **1b** with Ni^{II} and Mn^{II} (complexes **2b** and **4b**, respectively) are also reported. Surprisingly, **2b** forms dimers through short intermolecular Se···Se contacts in the solid state. Thus, **2b** is the only member of this family of binuclear metal complexes wherein the steric bulk of the $M(hfac)_2$ (hfac = 1,1,1,5,5,5-hexafluoroacetylacetonato) fragments does not inhibit the formation of dimers. Complex **4b**, however, does not form dimers in the solid state and has a crystal packing motif analogous to **4a**, resulting in similar magnetic behavior. Finally, mononuclear coordination species of **1a** with Ni^{II}, Co^{II}, and Mn^{II} are presented (**6a**, **7a**, and **8a**, respectively). Both **6a** and **7a** form dimers via short S···S contacts in the solid state. Although **8a** was isolated, the crystal structure could not be obtained. Instead, an unusual cocrystallization of the binuclear manganese(II) coordination complex and the mononuclear manganese(II) coordination complex ([**4a**][**8a**]$_2$ = **8a′**) was the only crystallographically identifiable species that could be obtained under our preparation conditions. Interestingly, a crystallographically analogous mixture **5a′** of mononuclear and binuclear zinc(II) coordination species was identified as a side product in the preparation of **5a**.

EXPERIMENTAL SECTION

General Considerations. All reactions and manipulations were performed under an argon atmosphere using standard Schlenk techniques. Solvents were dried and distilled under argon prior to use: tetrahydrofuran (THF) dried over sodium/benzophenone ketyl; methylene chloride dried over CaH_2; acetonitrile dried over P_2O_5. The $(bpym)Co_2(hfac)_4$ complex (bpym = 2,2′-bipyrimidine; hfac = 1,1,1,5,5,5-hexafluoroacetylacetonato) was prepared according to literature procedures.[6,7] The syntheses of 4-(2′-pyrimidyl)-*N*,*N*,*N*′-tris(trimethylsilyl)amidine, ligand **1a**, and manganese complex **4a** have been reported in our preliminary communication.[5] Metal bis-(hexafluoroacetylacetonato)dihydrates [$M(hfac)_2{\cdot}2H_2O$, where M = Ni^{II}, Co^{II}, Mn^{II}, and Zn^{II}] were prepared following a standard literature method[8] and, prior to use, were converted to anhydrous $M(hfac)_2{\cdot}2THF$ following previously employed methods[9] with the following slight modification: sodium sulfate was added to the warm THF solution and then removed by filtration prior to recovery of the product. Selenium tetrachloride was prepared according to a literature procedure.[10] All other reagents were purchased from Aldrich and used as received. IR spectra were recorded as pressed KBr pellets on a Nicolet 510-FTIR spectrometer at ambient temperature. Elemental analyses were performed at MHW Laboratories, Phoenix, AZ. Electron paramagnetic resonance (EPR) spectra were recorded on a Brüker EMX spectrometer. Electrochemical measurements were obtained at ambient temperature using an Autolab PGSTAT 30 instrument and a three-electrode (platinum) glass cell, sealed under an argon atmosphere.

4-(2′-Pyrimidyl)-1,2,3,5-diselenadiazolium Chloride ([pymDSDA$^+$][Cl$^-$]). Following an established route for the preparation of DSDA cation chlorides,[11] a solution of 4-(2′-pyrimidyl)-*N*,*N*,*N*′-tris(trimethylsilyl)amidine (1.1072 g, 3.2988 mmol) in 10 mL of acetonitrile was added to a solution of $SeCl_2$ [generated in situ from $SeCl_4$ (0.6588 g, 2.984 mmol) and Se powder (0.2473 g, 3.132 mmol)] in 20 mL of acetonitrile and heated gently for 1 h. The resulting orange powder was filtered and washed with 3 × 5 mL of acetonitrile and dried in vacuo to afford the title compound, which was used without further purification. Crude yield: 0.7026 g (69% based on amidine). ν_{max}(KBr)/cm^{-1}: 3123(w), 3056(w), 3029(w), 3018(w), 2974(w), 2958(w), 1695(w), 1561(s), 1418(m), 1373(m), 1358(m), 1262(w), 1188(m), 1177(m), 1100(w), 992(w), 845(w), 823(w), 781(m), 745(m), 714(w), 680(w), 661(w), 648(w), 631(m), 596(w), 449(w), 411(w).

4-(2′-Pyrimidyl)-1,2,3,5-diselenadiazolyl (pymDSDA; 1b). Solid triphenylantimony (2.0622 g, 5.8408 mmol) was added to a slurry of [**pymDSDA**$^+$][**Cl**$^-$] (3.5902 g, 11.489 mmol) in 100 mL of acetonitrile and refluxed for 1.5 h. The resulting black powder was filtered and washed with 3 × 20 mL of acetonitrile and dried in vacuo. Crude yield: 2.9619 g (94% based on [**pymDSDA**$^+$][**Cl**$^-$]). Crystals suitable for X-ray crystallography were obtained by dynamic vacuum sublimation (10^{-2} Torr) at 110 °C. ν_{max} (KBr)/cm^{-1}: 3122(w), 3058(w), 3028(w), 3018(w), 2977(w), 2964(w), 1736(w), 1557(s), 1435(w), 1418(s), 1345(m), 1270(w), 1256(w), 1226(w), 1180(m), 1106(w), 989(w), 968(w), 893(w), 877(w), 825(m), 798(w), 736(s), 723(s), 646(s), 632(s), 469(w), 426(w), 416(w). Anal. Calcd for $C_5H_3N_4Se_2$: C, 21.68; H, 1.09; N, 20.22. Found: C, 21.86; H, 1.31; N, 20.05. The solution X-band EPR spectrum (CH_2Cl_2, 295 K) consists of one broad, featureless absorption (spectral signal width of ca. 150 G), with g = 2.0382, consistent with similar DSDA radical species.[11] In the solid state, the magnetic susceptibility measurements reveal that **1b** is diamagnetic as expected on the basis of the strongly dimerized structure described below. The cyclic voltammetry of **1b** in CH_3CN (4 mM analyte; 0.18 M [nBu$_4$N][PF$_6$] electrolyte; the ferrocene/ferrocenium couple at $E_{1/2}$ = 0.40 V vs SCE as the internal standard[12]) reveals a reversible oxidative process $E_{1/2}$ = 0.79 V vs SCE (ΔE_{pp} = 120 mV) and a reductive process with poor chemical reversibility (cathodic peak potential E_{pc} = −0.76 V vs SCE; anodic peak potential E_{pa} = −0.59 V vs SCE).

(pymDTDA)Ni$_2$(hfac)$_4$ (2a). THF (10 mL) was added to a reaction vessel containing **1a** (0.0917 g, 0.500 mmol) and $Ni(hfac)_2{\cdot}2THF$ (0.6169 g, 0.9998 mmol), and the resulting solution was stirred at ambient temperature for 2 h. The solvent was removed in vacuo, and the recovered solid was purified by dynamic vacuum sublimation in a three-stage gradient-temperature tube furnace. Crude yield: 0.4523 g (0.4007 mmol, 80%). Green crystals suitable for crystallography and magnetic measurements were obtained by sublimation under a static vacuum at 140 °C (10^{-2} Torr). ν_{max} (KBr)/cm^{-1}: 1644(s), 1596(w), 1558(m), 1528(m), 1482(s), 1395(m), 1350(w), 1259(s), 1210(s), 1148(s), 1102(w), 858(w), 801(m), 745(w), 674(s), 649(w), 588(m), 529(w). Anal. Calcd for $C_{25}H_7F_{24}N_4Ni_2O_8S_2$: C, 26.60; H, 0.63; N, 4.96. Found: C, 26.80; H, 0.48; N, 4.82.

(pymDSDA)Ni$_2$(hfac)$_4$ (2b). A solution of $Ni(hfac)_2{\cdot}2THF$ (0.4466 g, 0.7238 mmol) in 20 mL of methylene chloride was added to a solution of **1b** (0.1044 g, 0.3768 mmol) in 300 mL of methylene chloride. The reaction mixture was stirred at room temperature for 40 min. The solvent was removed by flash distillation to give a dark solid residue, which was sublimed under a dynamic vacuum at 135 °C (10^{-2} Torr) to give small dark crystals. Crystals suitable for X-ray crystallography and magnetic measurements were

dx.doi.org/10.1021/ic3000284 | Inorg. Chem. 2012, 51, 3827−3839

obtained by static sublimation at 130 °C (10^{-3} Torr). ν_{max} (KBr)/cm^{-1}: 3145(w), 2961(w), 2914(w), 2847(w), 1642(s), 1594(w), 1557(m), 1530(m), 1472(s), 1370(m), 1350(w), 1257(s), 1203(s), 1148(s), 1098(w), 800(m), 766(w), 745(w), 674(s), 650(w), 588(m), 530(w). Anal. Calcd for $Ni_2(C_5H_3O_2F_6)_4(C_5H_3N_4Se_2)$: C, 24.56; H, 0.577; N, 4.582. Found: C, 24.82; H, 0.36; N, 4.39.

(pymDTDA)Co_2(hfac)$_4$ (3a). THF (10 mL) was added to a reaction vessel containing **1a** (0.1331 g, 0.7264 mmol) and 0.8978 g (1.455 mmol) of Co(hfac)$_2$·2THF. The resulting solution was stirred at ambient temperature for 2 h. The solvent was removed in vacuo, and the recovered solid was purified by dynamic vacuum sublimation in a three-stage gradient-temperature tube furnace. Crude yield: 0.6305 g (0.5583 mmol, 77%). Dark-purple crystals suitable for crystallography and magnetic measurements were obtained by sublimation under a static vacuum at 120 °C (10^{-2} Torr). ν_{max} (KBr)/cm^{-1}: 1641(s), 1595(w), 1585(w), 1563(m), 1529(m), 1487(m), 1454(w), 1390(s), 1348(w), 1322(w), 1259(s), 1207(s), 1148(s), 1098(w), 1018(w), 949(w), 855(w), 813(w), 797(m), 763(w), 743(w), 715(w), 670(s), 648(m), 586(s), 528(m). Anal. Calcd for $C_{25}H_7F_{24}Co_2N_4O_8S_2$: C, 26.59; H, 0.62; N, 4.96. Found: C, 26.34; H, 0.85; N, 4.81.

(pymDSDA)Mn_2(hfac)$_4$ (4b). Methylene chloride (120 mL) was distilled directly into a reaction flask containing **1b** (0.1106 g, 0.3992 mmol) to give a homogeneous golden solution to which a solution of Mn(hfac)$_2$·2THF (0.4903, 0.7995 mmol) in 15 mL of methylene chloride was delivered slowly via syringe. The resulting homogeneous red reaction mixture was allowed to stir at room temperature for 45 min, and the solvent was removed by flash distillation to leave a deep-blue residue. Crude yield: 0.3105 g (64% based on **1b**). Dark-red crystals, suitable for X-ray crystallography and magnetic measurements, were obtained by dynamic vacuum sublimation (10^{-2} Torr) at 135 °C. ν_{max} (KBr)/cm^{-1}: 3295(w), 3144(w), 2963(w), 2918(w), 2900(w), 2849(w), 1647(s), 1606(w), 1596(w), 1560(m), 1534(m), 1503(m), 1483(m), 1449(w), 1399(w), 1386(w), 1366(w), 1345(w), 1324(w), 1259(s), 1214(s), 1200(s), 1143(s), 1097(m), 1030(m), 948(w), 921(w), 873(w), 803(s), 775(w), 742(w), 665(s), 637(w), 586(m), 527(w), 465(w), 452(w), 439(w), 406(w). Anal. Calcd for $(C_5H_3N_4Se_2)Mn_2(C_5H_3O_2F_6)_4$: C, 24.71; H, 0.58; N, 4.61. Found: C, 24.60; H, 0.73; N, 4.51.

(pymDTDA)Zn_2(hfac)$_4$ (5a). A colorless solution of Zn(hfac$_2$)·2THF (1.4182 g, 2.2701 mmol) in 30 mL of methylene chloride was added to a dark-purple solution of **1a** (0.2023 g, 1.104 mmol) in 30 mL of methylene chloride. The resulting dark-blue solution was stirred at room temperature for 30 min. The solvent was removed by flash distillation, and the residue was divided into four portions, each of which was sublimed under a dynamic vacuum at 120 °C (10^{-1} Torr), yielding pale-blue blocks of **5a** [0.1322 g; 10% based on Zn(hfac$_2$)·2THF] suitable for X-ray crystallography and magnetic measurements. ν_{max} (KBr)/cm^{-1}: 2961(w), 2918(w), 2844(w), 1647(s), 1596(w), 1562(m), 1535(m), 1486(s), 1466(m), 1389(m), 1349(w), 1258(s), 1212(s), 1148(s), 1099(m), 1033(w), 948(w), 853(w), 802(m), 764(w), 744(w), 670(m), 647(w), 587(m), 529(w). Anal. Calcd for $C_{25}H_7F_{24}Zn_2N_4O_8S_2$: C, 26.28; H, 0.62; N, 4.91. Found: C, 26.10; H, 0.55; N, 4.72. The solution X-band EPR spectrum (CH_2Cl_2, 295 K) shows a 1:2:3:2:1 five-line pattern consistent with coupling to two equivalent ^{14}N nuclei; g = 2.010(6), a_N = 4.817 G. The coupling constant is slightly smaller than that observed in the free ligand.[5]

[(pymDTDA)Zn_2(hfac)$_4$][(pymDTDA)Zn(hfac)$_2$]$_2$ (5a′). Product **5a′** is prepared under essentially the same reaction conditions as **5a** with the exception of the use of a higher vacuum for sublimation. A typical procedure is as follows: A colorless solution of Zn(hfac$_2$)·2THF (1.0294 g, 1.6504 mmol) in 20 mL of methylene chloride was added to a dark-purple solution of **1a** (0.1693 g, 0.8186 mmol) in 30 mL of methylene chloride. The resulting dark-blue solution was stirred at room temperature for 30 min. The solvent was removed by flash distillation, and the residue was divided into two portions, each of which was sublimed under a dynamic vacuum at 120 °C (10^{-2} Torr), yielding dark-blue needles of **5a′** (0.2543 g; 27% yield based on Znhfac$_2$·2THF) suitable for X-ray crystallography and magnetic measurements. ν_{max} (KBr)/cm^{-1}: 3138(w), 2961(w), 2914(w), 2851(w), 1647(s), 1586(w), 1560(m), 1532(m), 1487(s), 1463(m), 1389(m), 1348(w), 1319(w), 1259(s), 1208(s), 1150(s), 1137(s), 1097(m), 861(w), 841(w), 813(m), 796(m), 763(w), 743(w), 716(w), 669(m), 647(w), 586(m), 526(w). Anal. Calcd for $C_{55}H_{17}F_{48}Zn_4N_{12}O_{16}S_6$: C, 26.76; H, 0.69; N, 6.81. Found: C, 27.12; H, 0.89; N, 6.75.

(pymDTDA)Ni(hfac)$_2$ (6a). THF (10 mL) was added to a mixture of Ni(hfac)$_2$·2THF (0.3046 g, 0.494 mmol) and **1a** (0.0906 g, 0.494 mmol), and the resulting solution was stirred for 1 h at room temperature. The solvent was removed by flash distillation, and 0.2651 g of a dark-purple powder was recovered. Dark-green crystals of **6a** (0.05061 g) suitable for X-ray crystallography were obtained by sublimation under a dynamic vacuum at 130 °C (10^{-2} Torr). ν_{max} (KBr)/cm^{-1}: 1642(s), 1584(m), 1558(m), 1529(m), 1483(s), 1391(s), 1348(w), 1258(s), 1198(s), 1150(s), 1100(m), 1052(w), 1019(w), 951(w), 873(m), 812(m), 797(s), 768(w), 744(m), 715(w), 673(s), 651(m), 588(m), 530(w), 470(w). Anal. Calcd for $C_{15}H_5F_{12}N_4NiO_4S_2$: C, 27.46; H, 0.77; N, 8.54. Found: C, 27.63; H, 0.65, N, 8.61.

(pymDTDA)Co(hfac)$_2$ (7a). THF (10 mL) was added to a mixture of Co(hfac)$_2$·2THF (0.3916 g, 0.634 mmol) and **1a** (0.1159 g, 0.634 mmol), and the resulting solution was stirred for 1 h at room temperature. The solvent was removed by flash distillation, and 0.3901 g of a dark-purple powder was recovered. Dark-red needle-shaped crystals of **7a** (0.0606 g) were obtained by sublimation under a dynamic vacuum at 120 °C (10^{-2} Torr). ν_{max} (KBr)/cm^{-1}: 1642(s), 1584(m), 1559(m), 1530(m), 1488(m), 1391(s), 1348(w), 1258(s), 1207(s), 1147(s), 1098(w), 949(w), 864(w), 799(s), 743(w), 714(w), 669(s), 649(m), 586(s), 528(m). Anal. Calc. dfor $C_{15}H_5CoF_{12}N_4O_4S_2$: C, 27.45; H, 0.77; N, 8.54. Found: C, 27.36; H, 0.49; N, 8.35.

(pymDTDA)Mn(hfac)$_2$ (8a) and [(pymDTDA)Mn_2(hfac)$_4$]-[(pymDTDA)Mn(hfac)$_2$]$_2$ (8a′). THF (10 mL) was added to a mixture of Mn(hfac)$_2$·2THF (1.0671 g, 1.73 mmol) and **1a** (0.3178 g, 0.1.73 mmol), and the resulting solution was stirred for 1 h at room temperature. The solvent was removed by flash distillation, and 1.1752 g of a dark-purple powder was recovered. Dark-purple microcrystals of **8a** (0.1942 g) were obtained by sublimation under a dynamic vacuum at 125 °C (10^{-2} Torr). A small number of olive-green crystals of **8a′** were also recovered under the same conditions. Repeated attempts at producing crystallographic quality samples of **8a** failed; however, a pure microcrystalline material was obtained and characterized. IR of **8a**, ν_{max}(KBr)/cm^{-1}: 1647(s), 1607(w), 1560(m), 1536(m), 1505(m), 1374(m), 1258(s), 1219(s), 1144(s), 1095(w), 1034(w), 874(w), 832(w), 803(m), 741(w), 666(s), 648(w), 527(w). Anal. Calcd for $C_{15}H_5F_{12}MnN_4O_4S_2$: C, 27.62; H, 0.77; N, 8.59. Found: C, 27.86; H, 0.60; N, 8.33.

Crystallographic Measurements of 2a, 3a, 5a, 5a′, 6a, 8a′, 1b, 2b, and 4b. Experimental details can be found in the Supporting Information.

Magnetic Measurements. Magnetic measurements were performed on polycrystalline samples of **1b**, **2a**, **2b**, **3a**, **4a**, **4b**, **5a**, and **5a′** (30.9, 22.1, 18.6, 29.5, 17.0, 29.4, 14.63, and 17.3 mg, respectively). The magnetic susceptibility measurements of all species except **5a** were obtained at the Centre de Recherche Paul Pascal in Bordeaux, France, with the use of a Quantum Design SQUID magnetometer MPMS-XL functioning between 1.8 and 400 K for direct-current (dc) applied fields ranging from −7 to +7 T. These samples were prepared in a glovebox under argon and sealed in a polyethylene bag (3 × 0.5 × 0.02 cm) in order to avoid any contact with air or water. The magnetic susceptibility measurements of **5a** were obtained at the BIMR at McMaster University in Hamilton, Ontario, Canada, with the use of a Quantum Design MPMS SQUID magnetometer functioning between 1.8 and 400 K for dc applied fields ranging from −5.5 to +5.5 T. The sample of **5a** was prepared in air and measured using a gel-cap sample holder. All magnetic data were corrected for the sample holder and diamagnetic contribution.

dx.doi.org/10.1021/ic3000284 | Inorg. Chem. 2012, 51, 3827−3839

RESULTS

Crystal Structures. As reported in our preliminary communication,[5] **1a** dimerizes in the cis-cofacial motif common to many 1,2,3,5-dithiadiazolyl (DTDA) radicals.[13,14] By contrast, the analogous selenazyl radical ligand **1b** forms dimers in the trans-cofacial motif (Figure 1). Interestingly, this

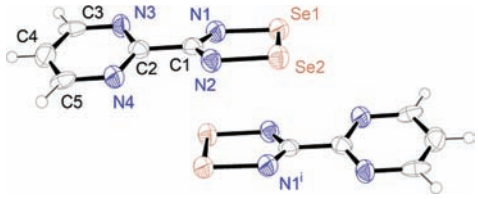

Figure 1. ORTEP image of **1b** showing the trans-cofacial dimers in the solid state (displacement ellipsoids at 50%). Symmetry code: (i) $-x$, $1-y$, $1-z$.

latter arrangement, while not uncommon for DTDA radicals,[15] is rarely observed for 1,2,3,5-diselenadiazolyl (DSDA) radicals. The distance between centroids of the DSDA rings at 150 K is 3.155(11) Å. Crystallographic information is provided in Table 1.

Binuclear coordination complexes **2a**, **3a**, and **5a** (Figure 2) are comprised of two $M(hfac)_2$ fragments (M = Ni, Co, and Zn, respectively) bridged by the DTDA ligand **1a**, resulting in molecular structures similar to that of the previously reported manganese(II) complex **4a**.[5] Crystallographic information and a select list of bond lengths are provided in Table 1. Complexes **2b** and **4b** (Figure 3) also have similar molecular structures (M = Ni and Mn, respectively) but incorporate the DSDA ligand **1b** (Table 1).

In this series of binuclear coordination complexes, the coordination geometry about the metal site is approximately the same for the nickel(II) complexes **2a** and **2b**, the cobalt(II) complex **3a**, and the zinc(II) complex **5a**, all of which exhibit a roughly octahedral arrangement of the six coordination points about the metal center. This is to be expected from ligand-field stabilization arguments for d^8 and high-spin (hs) d^7 ions, although no such argument can be made for a d^{10} ion. By contrast, for manganese(II) complexes **4a** and **4b**, the arrangement of the six coordination points about the metal sites is better described as approximately trigonal, rather than octahedral, for both molecules in the asymmetric unit. This is not unusual for hs d^5 metal ions.

The most important aspect of the solid-state structures is the crystal packing. The crystal structures of the Co^{II}- and Zn^{II}DTDA complexes, **3a** and **5a**, are isomorphous. The nickel(II) complex **2a**, while not isomorphous to **3a** and **5a**, has a similar solid-state arrangement (Figure 4) such that there are no close contacts between the thiazyl S atoms or metal or O atoms of neighboring molecules. By contrast, the Ni^{II}DSDA complex **2b** forms dimers in the solid state via short Se···Se contacts [3.215(5) Å; trans-antarafacial dimerization motif; Figure 5].

The crystal structures of manganese(II) complexes **4a** and **4b** are isomorphous, and the packing is significantly different from that seen in any of the other binuclear complexes. It is worth describing this packing in some detail here because interpretation of the magnetic data (vide infra) relies heavily on understanding the intricacies of the crystal packing. The following details are for complex **4b**, bearing in mind that they relate equally well to complex **4a** if one recognizes that the Se atoms of the former are substituted by the S atoms in the latter.

There are two molecules in the asymmetric unit, and these are both disordered with respect to the orientation of the central ligand. This disorder is illustrated in Figure 6a by including all C, N, and Se atom positions. The "Mn1"-containing molecule (*Molecule 1*) packs with no close contacts between neighboring Se, Mn, or O atoms. By contrast, the "Mn2"-containing molecule (*Molecule 2*) forms linear arrays propagating in the [100] direction, and close contacts between a Se atom of one molecule and two of the O atoms of a neighboring molecule are possible [Se1_2···O21, 3.266(3) Å; Se1_2···O41, 3.055(3) Å; for **4a**, S62···O21, 3.262(5) Å; S62···O41, 3.135(5) Å]. Given the crystallographic disorder, there are, in fact, three possible ways in which these molecules can interact. Figure 6b illustrates one possible motif in which *Molecule 2* packs in a "head-to-tail" arrangement with Se···O contacts between all neighboring molecules in an infinite chain. By flipping the orientation of a pymDSDA ligand (Figure 6c), the result is a pairwise interaction of two neighboring molecules via two sets of Se···O close contacts, which is the second possible mode of interaction. This also gives rise to the third possible interaction, which is that neighboring molecules do not have any close Se···O contacts (labeled "chain termination" in Figure 6c).

Attempts to characterize the solid-state structures of mononuclear complexes **6a**, **7a**, and **8a** of the pymDTDA ligand (M = Ni, Co, and Mn, respectively) have met with limited success. Crystallographic quality crystals of the nickel complex **6a** were isolated, and the molecular structure includes the expected chelation of a Ni^{II} ion by the pymDTDA ligand (Figure 7 and Table 2). The complex forms dimers in the solid state via short intermolecular S···S contacts [3.058(2) Å; trans-antarafacial dimerization motif]. Multiple attempts at growing crystals of **7a** failed to produce a sample that yielded publishable crystallographic data. From the poor-quality data sets that were obtained, it appears that this mononuclear cobalt complex is also dimerized in the solid state, albeit in the twisted cofacial motif (Figure S1 in the Supporting Information).

The mononuclear manganese complex **8a** could only be isolated as a microcrystalline material of insufficient quality for single-crystal X-ray analysis. However, sublimation repeatedly yielded a small number of high-quality crystals of **8a′** wherein one molecule of the binuclear $(pymDTDA)Mn_2(hfac)_4$ complex is cocrystallized with two molecules of the mononuclear complex **8a** (Figure 8 and Table 2). Interestingly, **8a′** is isomorphous with **5a′**, which is a 2:1 cocrystallization of the mononuclear zinc complex with the binuclear zinc complex of pymDTDA, isolated when the sublimation conditions are altered from those used in the preparation of **5a**. In the solid-state structures of both **8a′** and **5a′**, there is disorder with respect to the orientation of the pymDTDA ligand in the binuclear species. The most interesting features, however, are the intermolecular close contacts. The mononuclear molecules are organized along the [010] direction via short intermolecular S···N contacts [**8a′**: S1···N2, 3.031(3) Å; S2···N2, 3.350(3) Å; S2···N4, 3.021(3) Å; **5a′**: S1···N2, 3.012(2) Å; S2···N2, 3.344(2) Å; S2···N4, 3.018(2) Å]. The geometry of these S–N contacts is not unlike those often observed in DTDA solids.[14] Comparing them to Rawson's classification of these electrostatic interactions,[16] the geometry is closest to the SN-I or SN-IV type but is strictly neither of these and may be considered a related but novel geometry, perhaps labeled as an

dx.doi.org/10.1021/ic3000284 | Inorg. Chem. 2012, 51, 3827–3839

Table 1. Summary of Crystallographic Data, Including Select Bond Distances (Å) for 1a–5a, 1b, 2b, and 4b

	1a[a]	2a	3a	4a[a]		5a	1b	2b	4b	
formula	$C_5H_3N_4S_2$	$C_{25}H_7F_{24}N_4Ni_2O_8S_2$	$C_{25}H_7F_{24}N_4Co_2O_8S_2$	$C_{25}H_7F_{24}N_4Mn_2O_8S_2$		$C_{25}H_7F_{24}N_4Zn_2O_8S_2$	$C_5H_3N_4Se_2$	$C_{25}H_7F_{24}N_4Ni_2O_8Se_2$	$C_{25}H_7F_{24}N_4Mn_2O_8Se_2$	
fw, g mol^{-1}	183.23	1128.815	1129.301	1121.35		1142.21	277.03	1222.69	1215.15	
cryst color	red	blue-green	red	olive		green	purple	purple	red-brown	
a, Å	7.1561(4)	23.5273(7)	21.358(2)	8.9148(14)		21.486(4)	9.1678(16)	10.620(2)	8.9576(5)	
b, Å	10.6746(5)	13.1703(4)	16.112(2)	12.209(2)		16.218(3)	10.2767(18)	14.630(3)	12.2520(7)	
c, Å	10.1407(7)	24.8471(8)	13.0378(14)	18.562(3)		13.036(3)	7.7130(13)	14.893(3)	18.6441(11)	
α, deg	90.00	90.00	90.00	96.563(10)		90.00	90.00	67.20(3)	96.563(4)	
β, deg	116.994(3)	97.903(2)	124.763(5)	91.913(10)		124.77(3)	101.622(7)	70.41(3)	91.865(4)	
γ, deg	90.00	90.00	90.00	110.860(9)		90.00	90.00	85.75(3)	110.633(4)	
V, Å^3	690.24(7)	7626.04	3685.8	1869.5(5)		3731.5(13)	711.8(2)	2005.5(7)	1896.52(19)	
space group	$P2_1/c$	$C2/c$	$C2/c$	$P\bar{1}$		$C2/c$	$P2_1/c$	$P\bar{1}$	$P\bar{1}$	
Z	4	8	4	2		4	4	2	2	
T, K	100(2)	150(2)	100(2)	100(2)		150(2)	150(1)	150(2)	150(2)	
data/restraints/param	1216/492/203	6724/0/642	3245/0/295	6570/0/541		3291/126/322	1555/0/100	7088/209/586	6646/260/647	
R, R_w (on F^2)	0.0411, 0.0882	0.0540, 0.1258	0.0582, 0.1448	0.0584, 0.0962		0.0533, 0.1169	0.0497, 0.1196	0.0598, 0.1559	0.0499, 0.1070	
				Molecule 1	*Molecule 2*				*Molecule 1*	*Molecule 2*
S–S	2.093(3) 2.086(3)	2.084(2)	2.093(3)	2.072(5)	2.073(5)	2.088(3)				
Se–Se							2.3495(11)	2.3373(12)	2.328(2)	2.324(2)
M–N_{pym}		2.089(4), 2.123(4)	2.167(4)	2.361(9) , 2.26(3)	2.245(8) , 2.36(2)	2.191(4)		2.096(5), 2.100(5)	2.342(11) , 2.29(3)	2.257(9) , 2.30(2)
M–$N_{D(T/S)DA}$		2.146(4) ,2.139(4)	2.205(4)	2.380(12) , 2.308(13)	2.247(12) , 2.463(11)	2.307(4)		2.105(5) ,2.087(6)	2.285(15) , 2.281(14)	2.262(11) , 2.350(11)

[a]Previously published work.[5]

dx.doi.org/10.1021/ic3000284 | *Inorg. Chem.* 2012, 51, 3827–3839

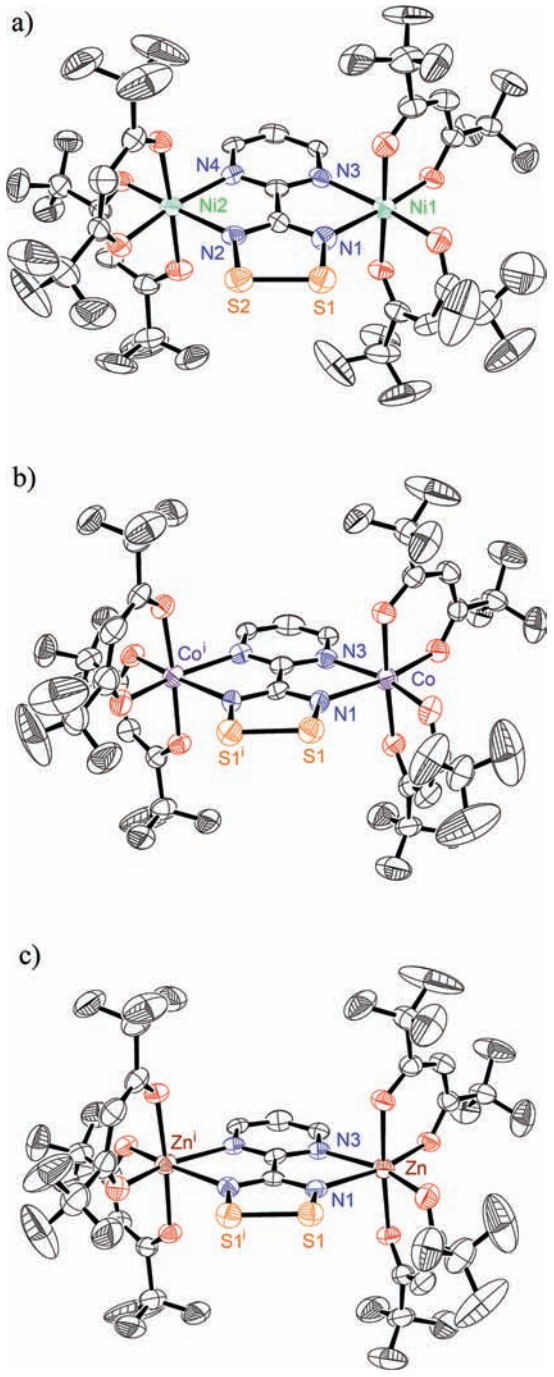

Figure 2. ORTEP depictions of the single-crystal X-ray structures of (a) complex **2a**, (b) complex **3a**, and (c) complex **5a**. Thermal ellipsoids at 50%; H atoms omitted. Symmetry code: (i) $-x, y, -(0.5 + z)$.

SN-V type (Figure 8). Furthermore, short chalcogen−oxygen contacts, similar to those observed in **4a** and **4b**, are also present in **8a′** and **5a′** between the binuclear molecules [**8a′**: S2_2···O61, 3.273(6) Å; S2_2···O75, 3.173(6) Å; **5a′**: S1_2···O65, 3.213(6) Å; S1_2···O71, 3.291(6) Å].

Magnetic Measurements. We have measured the dc magnetic susceptibilities of new binuclear complexes **2a**, **2b**, **3a**, **4b**, and **5a**. We have previously reported the solid-state magnetic properties of Mn^{II}DTDA complex **4a** and shown that the ground-state spin for a single molecule is $S_T = {}^9/_2$, owing to the AF coupling between the metal and ligand spins.[5] In the

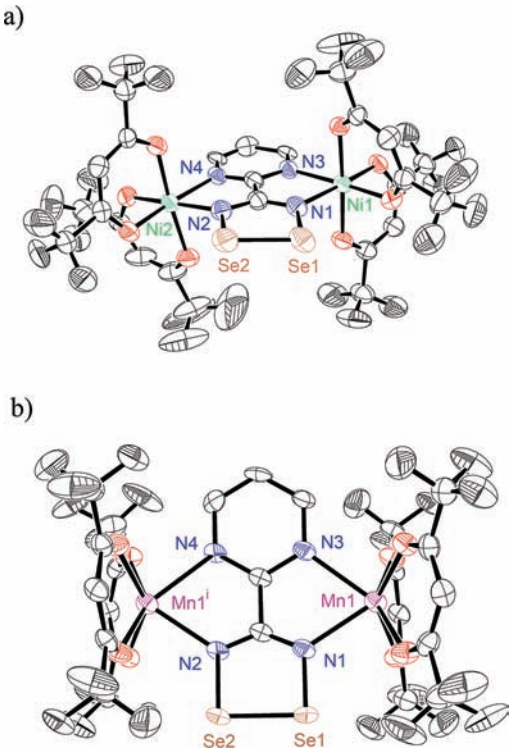

Figure 3. ORTEP depictions of the single-crystal X-ray structures of (a) complex **2b** and (b) one of two crystallographically unique molecules in the asymmetric unit of **4b**. Thermal ellipsoids at 50%; H atoms omitted. Symmetry code: (i) $1 - x, 2 - y, 1 - z$.

preliminary report, however, some questions remained as to the origin of the dramatic increase in the χT product at very low temperature. Herein we address this issue and present magnetic data for the new isomorphous Mn^{II}DSDA complex **4b**.

At room temperature, the χT product at 1000 Oe for **2a** and **2b** is 3.1 and 2.4 cm^3 K mol^{-1}, respectively (Figure 9). Upon a decrease in the temperature, the χT product for **2a** increases continuously to a maximum value of 4.2 cm^3 K mol^{-1} at 25 K, indicating dominant FM interactions between the Ni^{II} metal ions and the radical ligand DTDA, suggesting an $S_T = {}^5/_2$ spin ground state. The decrease of the χT product below 25 K and down to 1.8 K (1.9 cm^3 K mol) may be the result of weak AF interactions between complexes or the presence of magnetic anisotropy (zero-field splitting effects) arising from the Ni^{II} centers. On the basis of the structure, **2a** can be magnetically viewed as a spin trimer composed of two $S_{Ni} = 1$ and one $S_{DTDA} = {}^1/_2$ spin carriers. The magnetic data for complex **2a** can be modeled accordingly on the basis of an isotropic spin Heisenberg Hamiltonian, $\hat{H} = -2J(\hat{S}_{Ni1} + \hat{S}_{Ni2})\cdot\hat{S}_{DTDA}$, where J is the Ni···DTDA magnetic interaction and $\hat{S}_i$ are the spin operators. The theoretical expression of the magnetic susceptibility can be estimated by applying the van Vleck equation[17] to Kambe's vector coupling scheme[18] in the weak-field approximation:

$$\chi_0 = \frac{{g_{av}}^2 N {\mu_B}^2}{4k_B T} \times \frac{10 + e^{J/k_B T} + e^{3J/k_B T} + 10e^{4J/k_B T} + 35e^{5J/k_B T}}{2 + e^{J/k_B T} + e^{3J/k_B T} + 2e^{4J/k_B T} + 3e^{5J/k_B T}}$$

dx.doi.org/10.1021/ic3000284 | Inorg. Chem. 2012, 51, 3827−3839

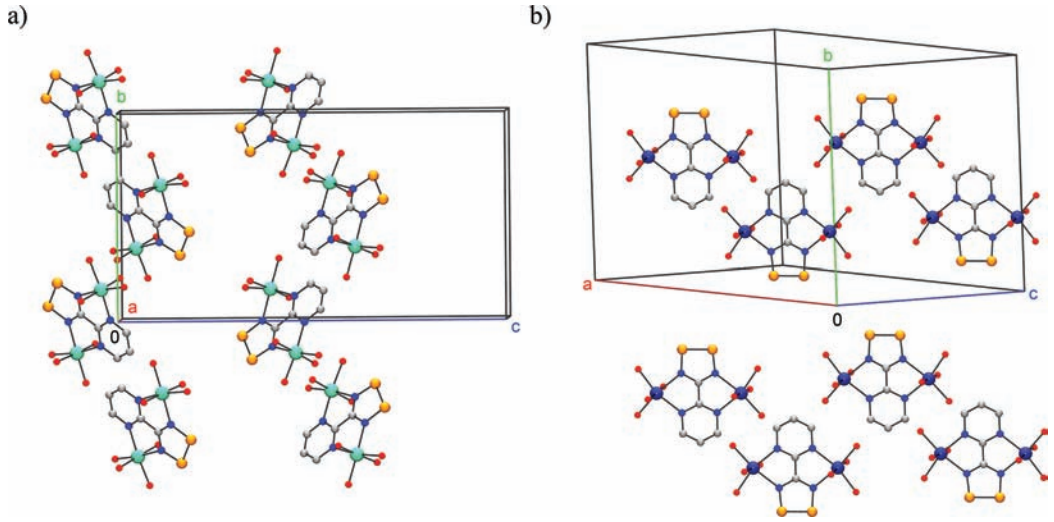

Figure 4. Crystal packing of (a) nickel(II) complex **2a** and (b) cobalt(II) complex **3a**. H atoms are omitted, and only the O atoms of the hfac ligands are shown. The crystal structure of zinc(II) complex **5a** is isomorphous to that of **3a**.

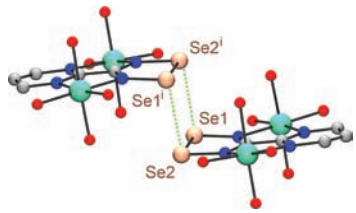

Figure 5. Crystal packing of nickel(II) complex **2b** illustrating the formation of dimers via short intermolecular Se···Se contacts [3.215(5) Å]. H atoms are omitted, and only the O atoms of the hfac ligands are shown. Symmetry code: (i) $1 - x, -y, 2 - z$.

In order to model the entire temperature range, intermolecular interactions have been introduced in the frame of the mean-field theory. The following definition of susceptibility has been used:

$$\chi = \frac{\chi_0}{1 - \frac{2zJ'}{N{g_{av}}^2{\mu_B}^2}\chi_0}$$

where χ_0 is the susceptibility of the noninteracting molecules, z is the number of nearest neighbors, and J' is the magnetic interaction between molecular units. An excellent model of the data (Figure 9) has been achieved using $J/k_B = +65(2)$ K, $zJ'/k_B = -0.45(5)$ K, and $g_{av} = 2.11(5)$, confirming the $S_T = {}^5/_2$ spin ground state of **2a**. It should be mentioned that when the Ni^{II} magnetic anisotropy is included in the model (using *MAGPACK* software to simulate the magnetic susceptibility),[19,20] the quality of the theory/experiment agreement does not improve and leads to undetermined zJ' and anisotropy parameters. As a consequence, the above value of zJ' should be considered as an upper limit of the intercomplex magnetic interactions because it also contains phenomenologically the Ni^{II} magnetic anisotropy.

In contrast, the χT product for **2b** is roughly constant down to 100 K and then decreases continuously to a minimum value of 0.9 cm^3 K mol^{-1} at 1.8 K, indicating weak but dominant AF interactions. This thermal behavior is likely the signature of only the Ni^{II} spin carriers because the DSDA radicals are strongly dimerized in the structure (vide supra), forming diamagnetic pairs. Therefore, the magnetic susceptibility of **2b** has been modeled accordingly on the basis of an isotropic spin Heisenberg Hamiltonian, $\hat{H} = -2J(\hat{S}_{Ni1}\cdot\hat{S}_{Ni2})$, where J is the Ni···Ni magnetic interaction through the diamagnetic DSDA molecule and $\hat{S}_{Ni}$ are the Ni^{II} spin operators. The theoretical expression of the magnetic susceptibility in the weak-field approximation is thus[21]

$$\chi_0 = \frac{{g_{av}}^2 N{\mu_B}^2}{k_B T}\,\frac{2e^{2J/k_BT} + 10e^{6J/k_BT}}{1 + 3e^{2J/k_BT} + 5e^{6J/k_BT}}$$

A good model of the data (Figure 9) down to 15 K has been obtained using $J/k_B = -4.3(5)$ K and $g_{av} = 2.23(5)$, confirming the absence of magnetic contribution from the DSDA paired radicals and also their singlet ground state.

The room temperature χT product of the cobalt(II) complex **3a** is 6.5 cm^3 K mol^{-1} (Figure 10). When the temperature is decreased at an applied field of 1000 Oe, the χT product decreases continuously to a minimum value of 5.7 cm^3 K mol^{-1} at approximately 42 K and then increases to a maximum value of 6.4 cm^3 K mol^{-1} at 6.1 K. Upon further cooling, the χT product decreases to a final minimum of 5.3 cm^3 K mol^{-1} at 1.8 K.

The Co^{II} metal ions possess a significant spin−orbit coupling that makes the magnetism of Co^{II}-based complexes difficult to analyze because no analytical expression is clearly established. Therefore, in order to gain insight into the interaction between the Co^{II} centers and the radical ligand, we have measured the magnetic susceptibility of $(bpym)Co_2(hfac)_4$ under the same conditions for comparison. The $(bpym)Co_2(hfac)_4$ complex is similar in structure to **3a**, but because bpym is a closed-shell ligand, the paramagnetic susceptibility arises entirely from the spin, spin−orbit coupling, and superexchange coupling of the two Co^{II} ions. Our data indicate that the room temperature χT product for $(bpym)Co_2(hfac)_4$ is 6.1 cm^3 K mol^{-1}, which is in good agreement with the published magnetic properties.[7] Using this value as a benchmark, the room temperature χT product of **3a** is reasonable for one radical ligand pymDTDA (expect 0.375 cm^3 K mol^{-1} for $g = 2$) plus two Co^{II} ions. A point-by-point subtraction of the χT product of $(bpym)Co_2(hfac)_4$ from the χT product of **3a** generates a plot (Figure 10) that represents the difference between these two species arising primarily from the inclusion of the radical ligand pymDTDA in place of the

dx.doi.org/10.1021/ic3000284 | *Inorg. Chem.* 2012, 51, 3827−3839

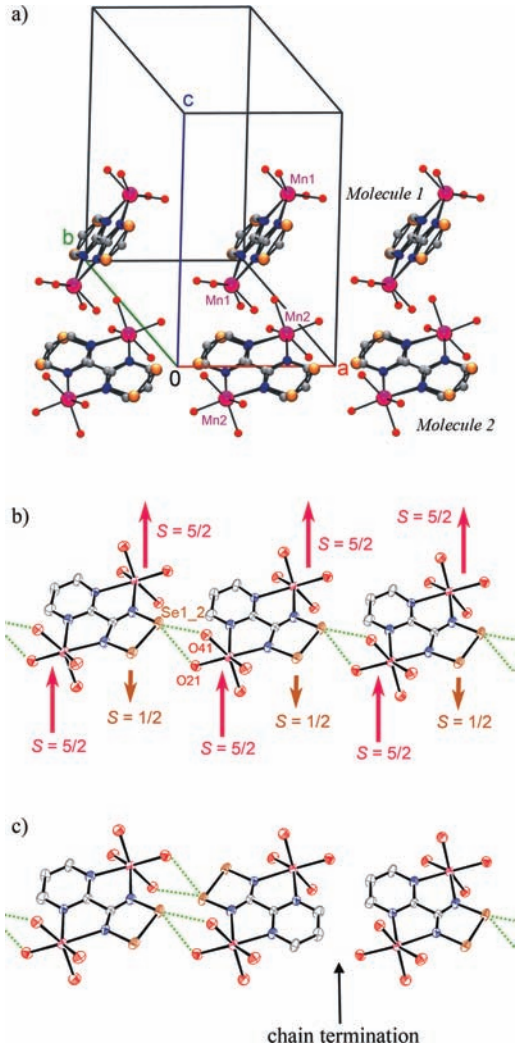

Figure 6. Crystal structure of manganese(II) complex **4b** (also representative of **4a**). H atoms are omitted, and only O atoms of the hfac ligands are shown. (a) Two crystallographically distinct molecules, both of which are disordered with respect to the orientation of the pymDSDA ligand. (b) Possible "head-to-tail" arrangement of *Molecule 2*. (c) Two other possible interactions involving *Molecule 2*. Short Se···O contacts indicated by dashed lines. The relative orientation of the spin vectors in the proposed ground-state configuration is indicated in part b.

closed-shell bpym ligand. This difference plot increases from room temperature down to 4 K, supporting a FM interaction between the Co^{II} ions and the pymDTDA radical. The observation of FM coupling is in agreement with a previously published mononuclear cobalt(II) complex of a similar DTDA-based radical ligand.[4] Below 4 K, the difference plot decreases with decreasing temperature. This may be a result of differences in any weak intermolecular interactions arising from crystal packing or small differences in the anisotropy of the two cobalt complexes.

We have previously reported the magnetic properties (χT) as a function of the temperature (300 to 2 K) at 1000 Oe for complex **4a**.[5] For our present purposes, in particular a comparison with **4b**, we have confirmed the reproducibility of this data. The analogous selenazyl complex **4b** has a solid-state structure isomorphous to **4a**; therefore, it is not surprising that the magnetic data have similar features. For **4b**, the χT

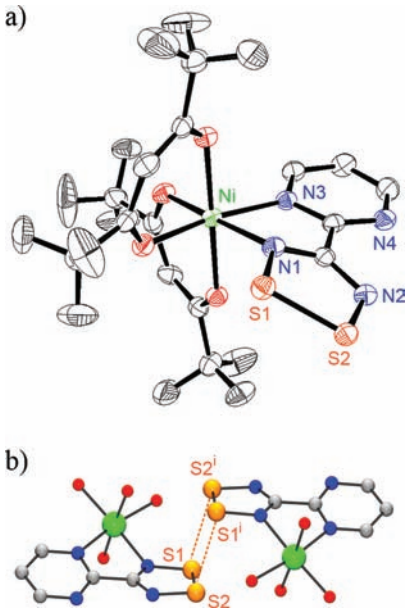

Figure 7. (a) ORTEP representation of **6a**. H atoms are omitted; thermal ellipsoids at 50%. (b) Dimer of **6a** complexes. Only the O atoms of the hfac ligands are included.

product (Figure 11) increases with decreasing temperature from a value of 8.1 cm^3 K mol^{-1} at 300 K to 12.5 cm^3 K mol^{-1} at 14 K. Upon further cooling to 6 K, the χT product increases up to 13.9 cm^3 K mol^{-1} at 1.8 K. The magnetic data from 300 to 6 K have been modeled on the basis of an isotropic spin Heisenberg Hamiltonian, $\hat{H} = -2J(\hat{S}_{Mn1} + \hat{S}_{Mn2})\cdot\hat{S}_{DSDA}$, treating the isolated molecule as a spin trimer composed of two $S_{Mn} = {}^5/_2$ and one $S_{DSDA} = {}^1/_2$. The theoretical expression of the magnetic susceptibility in the low field limit has been established from the van Vleck equation:[17]

$$\chi_0 = (g_{av}{}^2 N\mu_B{}^2/4k_BT)\{[286 + 165(e^{-11J/k_BT} + e^{-J/k_BT}) + 84(e^{-10J/k_BT} + e^{-2J/k_BT}) + 35(e^{-9J/k_BT} + e^{-3J/k_BT}) + 10(e^{-8J/k_BT} + e^{-4J/k_BT}) + (e^{-7J/k_BT} + e^{-5J/k_BT})]/[6 + 5(e^{-11J/k_BT} + e^{-J/k_BT}) + 4(e^{-10J/k_BT} + e^{-2J/k_BT}) + 3(e^{-9J/k_BT} + e^{-3J/k_BT}) + 2(e^{-8J/k_BT} + e^{-4J/k_BT}) + (e^{-7J/k_BT} + e^{-5J/k_BT})]\}$$

As for **4a**, in order to model the entire temperature range, effective intermolecular interactions have been introduced in the frame of the mean-field theory. Using this approach, the best least-squares fit of the experimental data (Figure 11) leads to $J/k_B = -50.9(5)$ K, $zJ'/k_B = +0.013(5)$ K, and $g_{av} = 1.98(5)$ for **4b**, which compares well with the values obtained for **4a**: $J/k_B = -30.2(5)$ K, $zJ'/k_B = +0.034(5)$ K, and $g_{av} = 1.99(5)$. The presence of strong AF coupling between the radical and the Mn^{II} spins induces an $S_T = {}^9/_2$ spin ground state for both complexes that is further confirmed by the fit of the M vs H/T data below 8 K for **4b** using an $S = {}^9/_2$ Brillouin function ($g = 2.01(2)$; Figure S2 in the Supporting Information).

dx.doi.org/10.1021/ic3000284 | *Inorg. Chem.* 2012, 51, 3827–3839

Table 2. Summary of Crystallographic Data, Including Select Bond Distances (Å) for 6a, 5a′, and 8a′

	6a	5a′		8a′	
formula	$C_{15}H_5F_{12}N_4NiO_4S_2$	$C_{55}H_{17}F_{48}N_{12}O_{16}S_6Zn_4$		$C_{55}H_{17}F_{48}Mn_4N_{12}O_{16}S_6$	
fw, g mol^{-1}	656.06	2467.65		2425.93	
cryst color	red	purple		orange	
a, Å	9.6479(8)	19.884(4)		19.8910(5)	
b, Å	9.9657(9)	8.8599(18)		8.8452(3)	
c, Å	12.3761(9)	23.216(5)		23.4215(5)	
α, deg	107.848(5)	90.00		90.00	
β, deg	100.353(5)	100.73(3)		101.026(2)	
γ, deg	100.592(4)	90.00		90.00	
V, Å^3	1077.36(15)	4018.4(14)		4044.71(19)	
space group	$P\bar{1}$	$P2_1/n$		$P2_1/n$	
Z	2	2		2	
T, K	100(0)	150(2)		100(2)	
data/restraints/param	4352/0/ 370	7095/274/677		7141/100/744	
R, R_w (on F^2)	0.0560, 0.1526	0.0509, 0.1188		0.0480, 0.1147	
		Mononuclear complex	*Binuclear complex*	*Mononuclear complex*	*Binuclear complex*
S–S	2.0837(15)	2.0898(19)	2.100(6)	2.0931(15)	2.074(6)
M–N_{pym}	2.072(3)	2.166(4)	2.203(16)	2.284(3)	2.366(8)
M–N_{DTDA}	2.101(3)	2.224(4)	2.117(16)	2.281(3)	2.453(13)

Below 6 K, the value of the χT product increases sharply to 13.9 cm^3 K mol^{-1} at 1.8 K for **4b**. This low temperature increase in χT beyond the expected value of 12.375 cm^3 K mol^{-1} for a single, isolated $S_T = {}^9/_2$ molecule has also been observed for **4a**, wherein the χT product reaches 14.0 cm^3 K mol^{-1} at 1.8 K. Given that the magnetoanisotropy is expected to be small for both **4a** and **4b**, it is reasonable to conclude that the increase in χT at low temperature is indicative of intermolecular exchange interactions that appear, at first glance, to be FM in nature on the basis of the positive sign of the zJ' parameters. This point will be further discussed in the Discussion section (vide infra).

Finally, we include the magnetic susceptibility measurements of **5a** and **5a′**. This is indeed the first report of a DTDA radical ligand coordinated to a diamagnetic metal ion. At 1000 Oe, the value of χT for **5a** is constant over the entire measured temperature range, indicating Curie behavior consistent with well-isolated spins (Figure 12). The Curie constant deduced from the Curie law fit shown in Figure 12 is 0.375 cm^3 K mol^{-1}, which is in very good agreement with the expected value for $S = {}^1/_2$ (g = 2.0).

The magnetic properties of **5a′** appear to be less straightforward. The room temperature χT product of **5a′** is 1.3 cm^3 K mol^{-1} (Figure 12) in agreement with the presence of three $S = {}^1/_2$ spins (two mononuclear and one binuclear molecules). When the temperature is decreased at an applied field of 1000 Oe, the χT product decreases continuously to a minimum value of 0.46 cm^3 K mol^{-1} at 1.8 K. The structure analysis reveals that the mononuclear molecules are organized in chains along b via short intermolecular S···N contacts, while the DTDA radical in the binuclear molecules appears globally well isolated thanks to the diamagnetic Zn metal ions. Therefore, because of the two types of radical sites, **5a′** can be viewed as a two-component magnetic system with (i) an $S = {}^1/_2$ chain along b that has been modeled to a regular AF quantum $S = {}^1/_2$ spin-chain model[22−24] (using the analytical expression of Bonner−Fisher for the chain and the following Hamiltonian definition: $H = -2J\sum_{i=1}^{N}\hat{S}_{DTDA,i}\cdot\hat{S}_{DTDA,i+1}$) in addition to (ii) an $S = {}^1/_2$ paramagnetic Curie contribution for the binuclear entities. The experimental data were fit relatively well down to 1.8 K with $J/k_B = -31.6(5)$ K and $g_{av} = 2.23(5)$ (Figure 12).

DISCUSSION

One of the purposes of creating radical ligands **1a** and **1b** is to take advantage of the highly directional coordination capabilities of a bis(bidentate) ligand that is structurally analogous to bpym and, by incorporating ligand-based spin, to add the element of strong, predictable mediation of magnetic coupling between metal centers. The idea is that, owing to the symmetry of the ligand in terms of both structure and spin distribution, the magnetic vectors of two identical chelated metal ions will align parallel to each other, regardless of the nature of the magnetic coupling with the ligand spin. If the metal spin couples ferromagnetically with the ligand spin, all of the magnetic vectors in the molecule align in parallel. If the metal spin couples antiferromagnetically with the ligand spin, the two metal spin vectors are still aligned parallel to each other in the overall ferrimagnetic scheme. The undimerized complexes of the DTDA and DSDA radical ligands with paramagnetic metal ions illustrate examples of both magnetic coupling scenarios: FM coupling for nickel(II) and cobalt(II) complexes **2a** and **3a** and AF coupling for manganese(II) complexes **4a** and **4b**.

Despite a small amount of magnetic anisotropy, the nickel(II) complex **2a** provides the most straightforward combination of structural and magnetic data. In the solid state, there are no close contacts between neighboring molecules through atoms with significant spin density, so it is reasonable to expect that the magnetic data arise predominantly from *intra*molecular exchange coupling between the nickel-based spin and the radical-ligand-based spin. These data support an $S_T = {}^5/_2$ spin ground state from FM interaction between two $S_{Ni} = 1$ and one $S_{DTDA} = {}^1/_2$, as might be predicted by a simple orbital overlap model.

The cobalt(II) complex **3a** is more difficult to analyze. Like complex **2a**, the crystal structure shows no close contacts between neighboring molecules via atoms with significant spin density. By contrast, it is expected that the magnetic data will be dominated by the large magnetic anisotropy of the Co^{II} ions.

dx.doi.org/10.1021/ic3000284 | Inorg. Chem. 2012, 51, 3827−3839

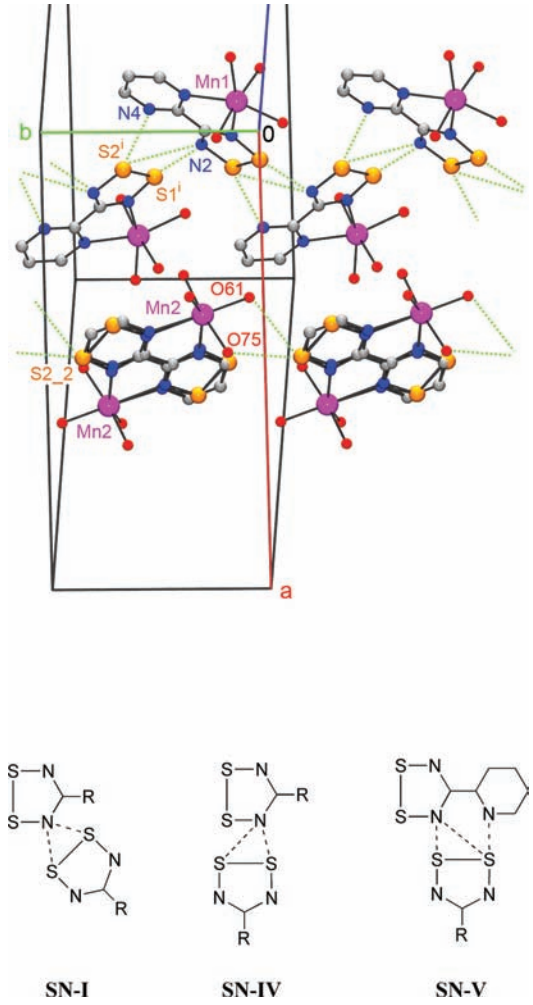

Figure 8. Top: Solid-state structure of the cocrystallized species **8a′**. H atoms are omitted; only O atoms of the hfac ligands are shown; crystallographic disorder is included; dotted lines represent close contacts. This is isomorphous with the zinc cocrystallized species **5a′** (not shown). Symmetry code: (i) $0.5 - x, y - 0.5, 0.5 - z$. Bottom: Rawson's[16] S···N interaction classifications SN-I and SN-IV and the proposed SN-V to represent the interactions observed in the **8a′** and **5a′** solids.

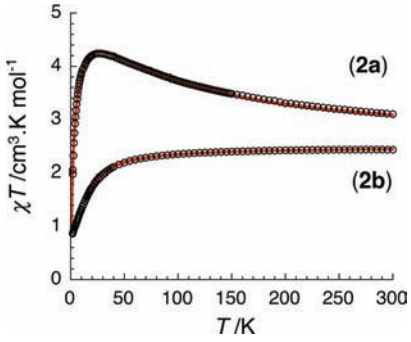

Figure 9. Temperature dependence of χT for nickel(II) complexes **2a** and **2b** at 1000 Oe (with χ defined as the magnetic susceptibility and equal to M/H per complex). Black circles indicate measured data, and the red lines represent the best least-squares fit obtained for the Heisenberg models described in the text down to 1.8 and 15 K for **2a** and **2b**, respectively.

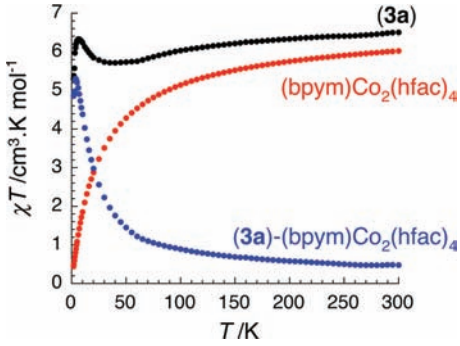

Figure 10. Temperature dependence of the χT product for cobalt(II) complex **3a** (black dots) and $(bpym)Co(hfac)_4$ (red dots) at 1000 Oe (with χ defined as the magnetic susceptibility and equal to M/H per complex). In blue dots is given the point-by-point subtraction of the χT values of the model complex $(bpym)Co(hfac)_4$ from the χT values of **3a** as a function of T.

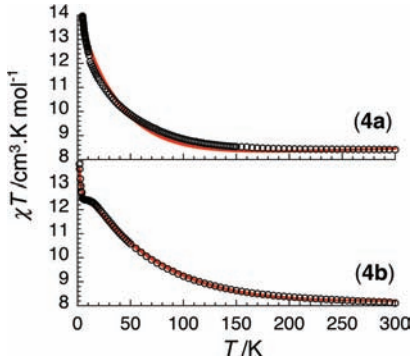

Figure 11. Temperature dependence of the χT product for manganese(II) complexes **4a** and **4b** at 1000 Oe (with χ defined as the magnetic susceptibility and equal to M/H per complex). Black circles indicate measured data, and the red lines represent the best least-squares fit obtained for the Heisenberg model described in the text.

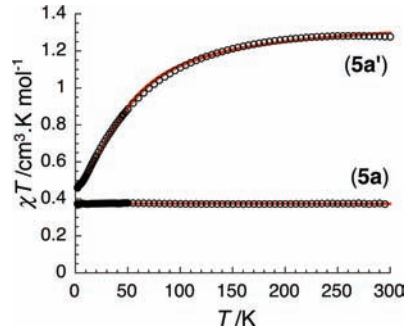

Figure 12. Temperature dependence of the χT product for zinc(II) complexes **5a** and **5a′** at 1000 Oe (with χ defined as the magnetic susceptibility and equal to M/H per complex). Black circles indicate measured data, and the red lines represent the best least-squares fit from the models described in the text.

Thus, in order to evaluate the nature of the magnetic interactions between the metal centers and the radical ligand, we have opted to measure the magnetic susceptibility of a model complex, $(bpym)Co_2(hfac)_4$, that has structural features similar to those of **3a**. Taking the point-by-point difference between the χT values of **3a** and the χT values of $(bpym)Co_2(hfac)_4$ produces a difference plot that is dominated

dx.doi.org/10.1021/ic3000284 | Inorg. Chem. 2012, 51, 3827−3839

by the ligand-based spin and the exchange coupling between the ligand and the two Co^{II} ions. Clearly, this is not a perfect subtraction of the contributions from magnetic anisotropy, metal-based spin, and superexchange between the metal centers, but the result is a reasonable illustration of the effect of the incorporation of the pymDTDA radical ligand **1a**. Furthermore, magnetic data obtained for the zinc(II) complex **5a**, which has a crystal structure analogous to that of **3a**, demonstrate that simple Curie behavior is to be expected from the coordinated ligand in the absence of a paramagnetic metal ion. Thus, the data for **3a** support an effective spin ground state of $S_T = {}^7/_2$ arising from FM coupling between two $S_{Co} = {}^3/_2$ and one $S_{DTDA} = {}^1/_2$.

The zinc(II) complexes **5a** and **5a′** are the first examples of a DTDA ligand coordinated to a diamagnetic metal ion. In the case of **5a** in particular, this serves to illustrate the magnetic properties of the coordinated paramagnetic ligand alone. This is especially informative as a benchmark for the analysis of magnetic data of species with large magnetic anisotropy, such as the cobalt(II) species **3a** (vide supra), and species with significant intermolecular interactions, such as the manganese(II) species **4a** (vide infra). In a comparison of **5a** and **5a′**, the addition of close intermolecular contacts between DTDA ligands of the mononuclear species in the latter have an obvious effect on the magnetic properties and serve to illustrate the importance of such contacts in general. It is particularly satisfying to note that the DTDA ligands are capable of mediating magnetic coupling between molecules without succumbing to dimer formation.

There is a very small number of other neutral, bis(bidentate) radical ligands, comparable to ligands **1a** and **1b**, in the literature. These are ligand designs based on oxoverdazyl radicals[25,26] and nitronyl nitroxides,[27] some of which are, in fact, diradical ligands. Our continuing interest in the development of radical ligands such as **1a** and **1b** from thiazyl and/or selenazyl heterocycles is founded on the observations that thiazyl radicals, and their selenium analogues, are known to order magnetically,[28−31] exhibit conductivity,[32−35] and exhibit bistability.[36−39] This wide range of possible solid-state behavior can generally be attributed to the absence of substituents on the thiazyl or selenazyl heteroatoms and the delocalization of the spin density over a large molecular area, which, as noted for **5a′**, may permit intermolecular interactions without the formation of diamagnetic dimers. In fact, the crystal engineering of DTDA and DSDA radical materials is currently a vibrant field of study,[14,40−46] as is the design and development of new thiazyl and selenazyl radicals for their solid-state electronic properties.[47−58] Thus, a second purpose in creating radical ligands **1a** and **1b** is to encourage ligand-based *inter*molecular interactions that are unlikely or impossible with other radical-ligand designs.

When we first reported the structure and magnetic properties of manganese(II) complex **4a**, we reported the unusual increase in χT values at low temperature but were unable to rationalize this observation on the basis of the molecular structure. Recently, we have discovered that short contacts between a S atom of the DTDA ring and an O atom of an hfac ligand provide a pathway for *inter*molecular AF interactions between the DTDA spin and the Mn^{II} spin in pairs of (boaDTDA)Mn(hfac)$_2$ complexes [boaDTDA = 4-(benzoxazol-2′-yl)-1,2,3,5-dithiadiazolyl].[59] Because the *intra*molecular exchange coupling between the DTDA and Mn^{II} spins of the coordinated metal ion is also AF ($S = 2$ for one molecule), the result is an "effective FM" interaction and an increase in the total spin ground state to $S_T = 4$ per pair. Upon close examination of the crystal structure of complex **4a**, we find that similar short S···O contacts are present. These provide the most likely pathway for *inter*molecular exchange coupling that gives rise to a dramatic increase in the observed χT product at low temperature. To date, the (boaDTDA)Mn(hfac)$_2$ complex and the manganese(II) complex **4a** are the only DTDA−metal complexes for which an increase in the χT product above that expected for a single molecule is observed at low temperature and both exhibit short S···O contacts in the solid state. It should be noted that the only other species exhibiting these short S···O contacts are the mixed mono- and binuclear structures of the zinc(II) and manganese(II) complexes, **5a′** and **8a′**, respectively, and that sufficient quantities of pure **8a′** suitable for magnetic measurements were not obtained.

The most interesting observation regarding the crystal structure of **4a** is that the disorder gives rise to three possible packing scenarios and, therefore, three possible magnetic scenarios. The first scenario is that *Molecule 2* packs in a "head-to-tail" array in which every molecule has one set of S···O contacts, with each of its nearest neighbors creating a 1D spin chain. The second scenario is that there is a pairwise interaction of neighboring molecules with two sets of S···O contacts, similar to the interactions observed for the boaDTDA complex. This naturally gives rise to the third possible scenario in which the nearest neighbors have no close S···O contacts. Thus, a more accurate picture of the actual packing motif in **4a** is one in which there are 1D "spin oligomers" of random chain length that may also include pairwise interactions and are interrupted by packing of neighboring molecules with no close S···O contacts. This gives a plausible explanation for the observation of the dramatic increase in the χT product, i.e., effective FM intercomplex interactions, that occurs for every measured sample of **4a**. Furthermore, this provides the first evidence that thiazyl radical ligands may be able to mediate magnetic coupling between metal complexes to generate high spin species.

One of the purposes behind the preparation and characterization of the selenazyl analogue **4b** was an attempt to manipulate the crystal packing of the binuclear manganese(II) complex. By replacing the S atoms with larger Se atoms, we speculated that we might be able to eliminate the crystallographic disorder, resulting in exclusively pairwise interactions or, alternatively, exclusively 1D chain interactions. However, the crystallographic disorder persists in **4b** and, as a result, the magnetic properties of **4b** are very similar to those of **4a**. The only significant difference is that, in **4b**, the value of χT plateaus at 12.4 cm^3 K mol^{-1} between 14 and 6 K before the onset of a sharp increase upon further cooling. This value is extremely close to the expected χT product (12.375 cm^3 K mol^{-1}) for an $S_T = {}^9/_2$ ground state for a single molecule. Such a plateau does not exist in the magnetic data of **4a** (Figure 11) as a result of weaker intermolecular coupling arising from the replacement of S with Se. Indeed, the magnitude of the AF interaction, J_{AF}, between radical molecule and neighboring Mn^{II} metal ions (see Figure 6c) can be roughly estimated to −0.28(2) and −0.11(4) K for **4a** and **4b**, respectively, based on the energy conservation principle from the effective FM interaction (zJ'): $J'S_T^2 = -J_{AF}S_{rad}S_{Mn}$ (with $z = 2$, $S_T = {}^9/_2$, $S_{rad} = {}^1/_2$, and $S_{Mn} = {}^5/_2$). The selenium analogue **4b** provides further evidence that the short chalcogen−oxygen contacts are, in fact, an important feature related to intermolecular AF interactions.

dx.doi.org/10.1021/ic3000284 | Inorg. Chem. 2012, 51, 3827−3839

Curiously, despite the significant steric bulk of the hfac ligands and the roughly octahedral coordination sphere of the metal ions, the Ni(II)DSDA complex **2b** provides the only example to date of dimerization in the solid state for these binuclear complexes (Figure 5). This may be a reflection of a greater propensity for dimer formation among DSDA species than DTDA species, a phenomenon that has been observed in solution[60] and that has been corroborated by theoretical studies.[61] This, in turn, highlights the importance of the chalcogen−oxygen close contacts in directing the crystal packing for the manganese(II) complexes **4a** and **4b**. In these manganese(II) species, the coordination geometry about the metal ions is relatively flexible because of a lack of ligand-field stabilization energy; hence, the steric bulk provided by the hfac ligands can be shifted such that it is lessened in the vicinity of the DTDA and DSDA heteroatoms. This could, in principle, increase a propensity for dimer formation, yet we observe the chalcogen−oxygen contacts instead.

It is worth noting that the binuclear complexes presented herein are generally robust, volatile species that can be isolated in high purity and in moderate-to-high yield by vacuum sublimation, despite their high molecular weight. Mononuclear coordination complexes **6a**, **7a**, and **8a** of the pymDTDA ligand **1a** are largely uninteresting because of dimerization in the solid state and poor crystal growth; however, the observation of mixed crystal structures **5a′** and **8a′**, containing both mono- and binuclear complexes, is interesting, particularly because they were prepared by vacuum sublimation. The mixed manganese(II) complex **8a′** is only observed when a reaction stoichiometry intended to prepare the mononuclear complex **8a** is used. By contrast, the mixed zinc(II) complex **5a′** is reproducibly observed if the crude product from the synthesis of the binuclear complex **5a** is subjected to a higher vacuum for sublimation. No evidence for this type of mixed crystal structure has been observed for any of the other metal ions. It is unclear whether the formation of the mono- and binuclear species incorporated in these mixed structures occurs during the synthesis or as a result of decomposition or rearrangement under sublimation conditions. It is equally unclear whether there is any straightforward reason that these mixed-metal systems are only observed for the d^{10} and hs d^5 metal ions.

CONCLUSION

Thiazyl and selenazyl radical ligands **1a** and **1b** can chelate two metal ions with supporting hfac ligands. The resulting complexes are robust and volatile such that they can be sublimed in good yield despite their high molecular weight. For the nickel(II) and cobalt(II) complexes of the thiazyl radical **1a** (**2a** and **3a**, respectively), the magnetic data confirm that the metal-based spin couples ferromagnetically to the ligand-based spin, giving rise to an $S_T = {}^5/_2$ spin ground state for **2a** and an $S_T = {}^7/_2$ spin ground state for **3a**. The previously reported manganese(II) complex **4a** has a spin ground state $S_T = {}^9/_2$ owing to AF coupling between the metal and DTDA spins; however, close intermolecular S···O contacts, albeit disrupted by crystallographic disorder, provide a pathway for intermolecular AF coupling between the metal and DTDA spins of neighboring molecules, giving rise to an increase in the χT product at low temperature. The analogous selenazylmanganese(II) complex **4b** has similar crystal packing and similar magnetic properties, with short Se···O contacts providing the intermolecular coupling pathway. These results demonstrate the capability of thiazyl and selenazyl radical ligands to mediate magnetic coupling between two coordinated metal ions and between neighboring metal complexes to generate high spin species.

The zinc(II) coordination complex **5a** provides benchmark magnetic data for a coordinated DTDA ligand in the absence of other paramagnetic species. Results regarding mononuclear coordination complexes **6a**, **7a**, and **8a** were largely uninteresting or uninformative. The observation of mixed mono- and binuclear complexes **5a′** and **8a′** is unexpected, as is the dimerization of the binuclear nickel(II) complex **2b** in the solid state.

ASSOCIATED CONTENT

Supporting Information

Crystallographic information files (CIF), details regarding crystallographic data collection and refinement for **1b**, **2a**, **2b**, **3a**, **4b**, **5a**, **5a′**, **6a**, and **8a′**, a figure of **7a** created from unpublishable crystallographic data, and additional magnetic data for **4b**. This material is available free of charge via the Internet at http://pubs.acs.org.

AUTHOR INFORMATION

Corresponding Author

*E-mail: kpreuss@uoguelph.ca.

Notes

The authors declare no competing financial interest.

ACKNOWLEDGMENTS

K.E.P. is grateful for funding from the Natural Sciences and Engineering Research Council of Canada in the form of a Discovery Grant, the Canada Foundation for Innovation Leaders Opportunity Fund, the Ontario Innovation Trust, the Canada Research Chairs program, and the University of Guelph. R.C. and I.-R.J. also thank the University of Bordeaux, the Région Aquitaine, the GIS Advanced Materials in Aquitaine (COMET Project), and the CNRS for financial support.

REFERENCES

(1) Hearns, N. G. R.; Clérac, R.; Jennings, M.; Preuss, K. E. *Dalton Trans.* **2009**, 3193.
(2) Hearns, N. G. R.; Fatila, E. M.; Clérac, R.; Jennings, M.; Preuss, K. E. *Inorg. Chem.* **2008**, *47*, 10330.
(3) Britten, J.; Hearns, N. G. R.; Preuss, K. E.; Richardson, J. F.; Bin-Salamon, S. *Inorg. Chem.* **2007**, *46*, 3934.
(4) Hearns, N. G. R.; Preuss, K. E.; Richardson, J. F.; Bin-Salamon, S. *J. Am. Chem. Soc.* **2004**, *126*, 9942.
(5) Jennings, M.; Preuss, K. E.; Wu, J. *Chem. Commun.* **2006**, 341.
(6) Brewer, G.; Sinn, E. *Inorg. Chem.* **1985**, *24*, 4580.
(7) Barquín, M.; González Garmendia, M. J.; Bellido, V. *Transition Met. Chem.* **1999**, *24*, 584.
(8) Belford, R. L.; Martell, A. E.; Calvin, M. *J. Inorg. Nucl. Chem.* **1956**, *2*, 11.
(9) Preuss, K. E.; Wu, J.; Jennings, M. *Acta Crystallogr.* **2005**, *E61*, M430.
(10) Yost, D. M.; Kircher, C. E. *J. Am. Chem. Soc.* **1930**, *52*, 4680.
(11) Del Bel Belluz, P.; Cordes, A. W.; Kristof, E. M.; Kristof, P. V.; Liblong, S. W.; Oakley, R. T. *J. Am. Chem. Soc.* **1989**, *111*, 9276.
(12) Connelly, N. G.; Geiger, W. E. *Chem. Rev.* **1996**, *96*, 877.
(13) Vegas, A.; Pérez-Salazar, A.; Banister, A. J.; Hey, R. G. *J. Chem. Soc., Dalton Trans.* **1980**, 1812.
(14) Haynes, D. A. *Cryst. Eng. Comm.* **2011**, *13*, 4793.
(15) Barclay, T. M.; Cordes, A. W.; George, N. A.; Haddon, R. C.; Itkis, M. E.; Oakley, R. T. *Chem. Commun.* **1999**, 2269.
(16) Bond, A. D.; Haynes, D. A.; Pask, C. M.; Rawson, J. M. *J. Chem. Soc., Dalton Trans.* **2002**, 2522.

(17) van Vleck, J. H. *The Theory of Electric and Magnetic Susceptibility*; Oxford University Press: London, 1932.
(18) Kambe, K. *J. Phys. Soc. Jpn.* **1950**, *5*, 48.
(19) Borrás-Almenar, J. J.; Clemente-Juan, J. M.; Coronado, E.; Tsukerblat, B. S. *Inorg. Chem.* **1999**, *38*, 6081.
(20) Borrás-Almenar, J. J.; Clemente-Juan, J. M.; Coronado, E.; Tsukerblat, B. S. *Comput. Chem.* **2001**, *22*, 985.
(21) O'Connor, C. J. *Prog. Inorg. Chem.* **1982**, *29*, 203.
(22) Bonner, J. C.; Fisher, M. E. *Phys. Rev.* **1964**, *135*, A640.
(23) Estes, W. E.; Gavel, D. P.; Hatfield, W. E.; Hodgson, D. J. *Inorg. Chem.* **1978**, *17*, 1415.
(24) Hall, J. W.; Marsh, W. E.; Weller, R. R.; Hatfield, W. E. *Inorg. Chem.* **1981**, *20*, 1033.
(25) Brook, D. J. R.; Lynch, V.; Conklin, B.; Fox, M. A. *J. Am. Chem. Soc.* **1997**, *119*, 5155.
(26) Barclay, T. M.; Hicks, R. G.; Lemaire, M. T.; Thompson, L. K. *Inorg. Chem.* **2001**, *40*, 5581.
(27) Tanaka, M.; Matsuda, K.; Itoh, T.; Iwamura, H. *Angew. Chem., Int. Ed.* **1998**, *37*, 810.
(28) Banister, A. J.; Bricklebank, N.; Lavender, I.; Rawson, J. M.; Gregory, C. I.; Tanner, B. K.; Clegg, W.; Elsegood, M. R. J.; Palacio, F. *Angew. Chem., Int. Ed.* **1996**, *35*, 2533.
(29) Alberola, A.; Less, R. J.; Pask, C. M.; Rawson, J. M.; Palacio, F.; Oliete, P.; Paulsen, C.; Yamaguchi, A.; Farley, R. D.; Murphy, D. M. *Angew. Chem., Int. Ed.* **2003**, *42*, 4782.
(30) Robertson, C. M.; Myles, D. J. T.; Leitch, A. A.; Reed, R. W.; Dooley, B. M.; Frank, N. L.; Dube, P. A.; Thompson, L. K.; Oakley, R. T. *J. Am. Chem. Soc.* **2007**, *129*, 12688.
(31) Robertson, C. M.; Leitch, A. A.; Cvrkalj, K.; Myles, D. J. T.; Reed, R. W.; Dube, P. A.; Oakley, R. T. *J. Am. Chem. Soc.* **2008**, *130*, 14791.
(32) Leitch, A. A.; Yu, X.; Winter, S. M.; Secco, R. A.; Dube, P. A.; Oakley, R. T. *J. Am. Chem. Soc.* **2009**, *131*, 7112.
(33) Tse, J. S.; Leitch, A. A.; Yu, X.; Bao, X.; Zhang, S.; Liu, Q.; Jin, C.; Secco, R. A.; Desgreniers, S.; Ohishi, Y.; Oakley, R. T. *J. Am. Chem. Soc.* **2010**, *132*, 4876.
(34) Yu, X.; Mailman, A.; Dube, P. A.; Assoud, A.; Oakley, R. T. *Chem. Commun.* **2011**, *47*, 4655.
(35) Leitch, A. A.; Lekin, K.; Winter, S. M.; Downie, L. E.; Tsuruda, H.; Tse, J. S.; Mito, M.; Desgreniers, S.; Dube, P. A.; Zhang, S.; Liu, Q.; Jin, C.; Ohishi, Y.; Oakley, R. T. *J. Am. Chem. Soc.* **2011**, *133*, 6051.
(36) Fujita, W.; Awaga, K. *Science* **1999**, *286*, 261.
(37) Fujita, W.; Awaga, K. *Synth. Met.* **2003**, *137*, 1263.
(38) Brusso, J. L.; Clements, O. P.; Haddon, R. C.; Itkis, M. E.; Leitch, A. A.; Oakley, R. T.; Reed, R. W.; Richardson, J. F. *J. Am. Chem. Soc.* **2004**, *126*, 8256.
(39) Awaga, K.; Tanaka, T.; Shirai, T.; Fujimori, M.; Suzuki, Y.; Yoshikawa, H.; Fujita, W. *Bull. Chem. Soc. Jpn.* **2006**, *79*, 25.
(40) Feeder, N.; Less, R. J.; Rawson, J. M.; Oliete, P.; Palacio, F. *Chem. Commun.* **2000**, 2449.
(41) Beer, L.; Cordes, A. W.; Myles, D. J. T.; Oakley, R. T.; Taylor, N. J. *Cryst. Eng. Comm.* **2000**, *2*, 109.
(42) Britten, J. F.; Clements, O. P.; Cordes, A. W.; Haddon, R. C.; Oakley, R. T.; Richardson, J. F. *Inorg. Chem.* **2001**, *40*, 6820.
(43) Alberola, A.; Clarke, C. S.; Haynes, D. A.; Pascu, S. I.; Rawson, J. M. *Chem. Commun.* **2005**, 4726.
(44) Allen, C.; Haynes, D. A.; Pask, C. M.; Rawson, J. M. *Cryst. Eng. Comm.* **2009**, *11*, 2048.
(45) Clarke, C. S.; Haynes, D. A.; Smith, J. N. B.; Batsanov, A. S.; Howard, J. A. K.; Pascu, S. I.; Rawson, J. M. *Cryst. Eng. Comm.* **2010**, *12*, 172.
(46) Alberola, A.; Carter, E.; Constantinides, C. P.; Eisler, D. J.; Murphy, D. M.; Rawson, J. M. *Chem. Commun.* **2011**, *47*, 2532.
(47) Rawson, J. M.; Alberola, A.; Whalley, A. *J. Mater. Chem.* **2006**, *16*, 2560.
(48) Decken, A.; Ebdah, M.; Kowalczyk, R. M.; Landee, C. P.; McInnes, E. J. L.; Passmore, J.; Shuvaev, K. V.; Thompson, L. K. *Inorg. Chem.* **2007**, *46*, 7756−7766.
(49) Alberola, A.; Clements, O. P.; Collis, R. J.; Cubbitt, L.; Grant, C. M.; Less, R. J.; Oakley, R. T.; Rawson, J. M.; Reed, R. W.; Robertson, C. M. *Cryst. Growth Des.* **2008**, *8*, 155.
(50) Awaga, K.; Umezono, Y.; Fujita, W.; Yoshikawa, H.; Cui, H.; Kobayashi, H.; Staniland, S. S.; Robertson, N. *Inorg. Chim. Acta* **2008**, *361*, 3761.
(51) Winter, S. M.; Cvrkalj, K.; Dube, P. A.; Robertson, C. M.; Probert, M. R.; Howard, J. A.; Oakley, R. T. *Chem. Commun.* **2009**, 7306.
(52) Iwasaki, A.; Hu, L.; Suizu, R.; Nomura, K.; Yoshikawa, H.; Awaga, K.; Noda, Y.; Kanai, K.; Ouchi, Y.; Seki, K.; Ito, H. *Angew. Chem.* **2009**, *48*, 4022.
(53) Alberola, A.; Eisler, D.; Less, R. J.; Navarro-Moratalla, E.; Rawson, J. M. *Chem. Commun.* **2010**, *46*, 6114.
(54) Lekin, K.; Winter, S. M.; Downie, L. E.; Bao, X.; Tse, J. S.; Desgreniers, S.; Secco, R. A.; Dube, P. A.; Oakley, R. T. *J. Am. Chem. Soc.* **2010**, *132*, 16212.
(55) Cameron, T. S.; Decken, A.; Grein, F.; Knapp, C.; Passmore, J.; Rautiainen, J. M.; Shuvaev, K. V.; Thompson, R. C.; Wood, D. J. *Inorg. Chem.* **2010**, *49*, 7861.
(56) Decken, A.; Mailman, A.; Passmore, J.; Rautiainen, J. M.; Scherer, W.; Scheidt, E. W. *Dalton Trans.* **2011**, *40*, 868.
(57) Alberola, A.; Eisler, D. J.; Harvey, L.; Rawson, J. M. *Cryst. Eng. Comm.* **2011**, *13*, 1794.
(58) Shuku, Y.; Suizu, R.; Awaga, K. *Inorg. Chem.* **2011**, *50*, 11859.
(59) Fatila, E. M.; Goodreid, J.; Clérac, R.; Jennings, M.; Assoud, J.; Preuss, K. E. *Chem. Commun.* **2010**, *46*, 6569.
(60) Davies, J. E.; Less, R. J.; May, I.; Rawson, J. M. *New J. Chem.* **1998**, 763.
(61) Cordes, A. W.; Bryan, C. D.; Davis, W. M.; Delaat, R. H.; Glarum, S. H.; Goddard, J. D.; Haddon, R. C.; Hicks, R. G.; Kennepohl, D. K.; Oakley, R. T.; Scott, S. R.; Westwood, N. P. C. *J. Am. Chem. Soc.* **1993**, *115*, 7232.